

Experimental study on seismic performance of coupling beams not designed for ductility

S.S.E. Lam[†]

Department of Civil and Structural Engineering, The Hong Kong Polytechnic University, Hong Kong

B. Wu[‡]

Department of Civil Engineering, South China University of Technology, Guangzhou, China

Z.Q. Liu^{‡†}

School of Civil Engineering, Harbin Institute of Technology, Harbin, China

Y.L. Wong^{‡‡}

Department of Civil and Structural Engineering, The Hong Kong Polytechnic University, Hong Kong

(Received April 10, 2006, Accepted November 27, 2007)

Abstract. Seismic performance of coupling beams not designed for ductility is examined. Eight 1:4 scale coupling beam specimens, with seven reinforced concrete sections and one composite section, were tested under cycles of push-pull action. Characteristics of the specimens include moderate shear span ratio in the range of 2.5-3.5, high main reinforcement ratio at 3-4% and small to large stirrup spacing with 90-degree hooks. All the reinforced concrete specimens failed in a brittle manner. Displacement ductility of specimens with large stirrup spacing (≥ 140 mm) is in the range of 3 to 5. Seismic performance of the specimens is also examined using the ultimate drift angle and the amount of energy dissipated. Correlating the test data, an empirical relationship is proposed to estimate the ultimate drift angle of a class of coupling beams considered in the study not designed for ductility.

Keywords: reinforced concrete; coupling beams; seismic; shear; ultimate drift angle; ductility.

1. Introduction

In regions without seismic provisions, reinforced concrete buildings can be designed based on strength and without consideration on ductility, in accordance with, say the BS8110:1985. Recent

[†] Associate Professor, Corresponding author, E-mail: cesslam@polyu.edu.hk

[‡] Professor

^{‡†} Research Student

^{‡‡} Associate Professor

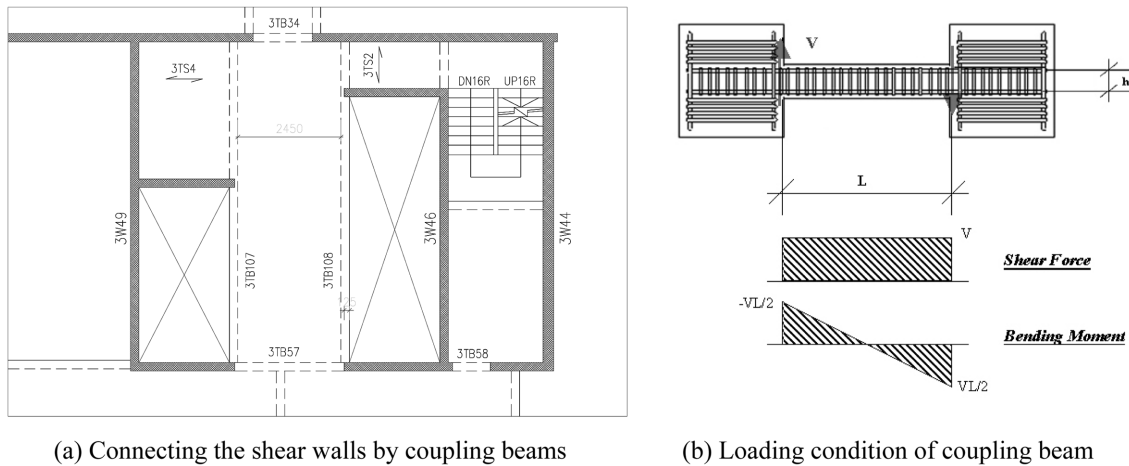


Fig. 1 Example of coupling beams and loading condition

worldwide seismic activities have led to the reassessment of the seismic risks in some regions. For instance, Hong Kong traditionally accepted as a region without seismic risk is now being recognized as a region of moderate seismic risk, Xu *et al.* (2001). When subjected to seismic attack, there could be interruption to critical facilities and business operations. This may lead to serious social and economical consequences. Among others, Durrani *et al.* (1995) predicted the performance of non-ductile flat slab systems with discontinuous bottom reinforcements at supports. Aycardi (1994) and Bracci and Reinhorn (1996) conducted experimental studies on non-ductile frames. Pam *et al.* (2002) examined the seismic resistant of beam-column joints designed to non-seismic requirements. Lam *et al.* (2003) quantified the ductility and ultimate drift ratio of reinforced concrete columns with high axial load and without sufficient confinement.

In high-rise buildings, it is common to couple reinforced concrete shear walls through the use of beams with moderate shear span ratio (typical in the range of 2.5 to 3.5). This type of beam is better known as the coupling beams. Fig. 1(a) shows part of the typical floor plan of a high-rise commercial building. To provide an efficient structural system, the two lift cores are connected by coupling beams (3TB34 and 3TB57). Typical clear span of the beams is 2.5 m to 3.0 m and with a structural depth about 750 mm. The end shears to be resisted by the coupling beams varied along the height of the building. The critical coupling beam is usually at a story about $H/3$ from the ground, where H is the height of building. Since geometries of the coupling beams remain the same throughout the typical floors, the critical coupling beam will have to be designed against an extreme shear force.

For seismic design of conventionally reinforced coupling beams, the design is based on flexural and shear requirements of beams if the shear span ratio is greater than some specified value. According to ACI318-02, when shear span ratio is less than 1 and the factored shear force exceeding certain value, the coupling beams have to be diagonally reinforced. When the shear span ratio is greater than 2 (i.e., the cases considered in this study), the requirements follow the provisions for flexural members of special moment frames. Similar guidelines are also given in NZS 3101:2006 Part 1.

Paulay (1997) examined the behavior of coupling beams with shear span ratios at 0.51 and 0.65. The study has indicated that cyclic behavior of relatively deep coupling beams does not follow the

conventional concept of double-curvature bending. Similar conclusion was also reached by Subedi (1991a,b). Paulay and Binney (1974) introduced the use of diagonal bars as main reinforcement to resist simultaneous moment and shear over the entire span. Barney *et al.* (1986) tested diagonally reinforced coupling beams with shear span ratio between 1.25 and 2.5. The study confirmed the effectiveness of such reinforcement details. Tassios *et al.* (1996) examined the performance of short coupling beams with different reinforcement layouts. Harries *et al.* (1996) considered the design requirements on different types of coupling beams. Harris (2001) reviewed previous investigations on coupling beams. This study also serves to indicate that coupling beams with shear span ratio between 2.5 and 3.5 were not considered in previous studies. Paulay (2002) provided means to estimate the deformation capacity of reinforced concrete coupled shear wall system. Demand of coupling beams were quantified by the drift angle and an example of a coupled core wall structure with shear span ratio of the coupling beams at 1.67 was presented. Hindi and Hassan (2004) proposed a theoretical model to predict the monotonic load-deformation behavior of diagonally reinforced coupling beams. Recently, Hindi and Hassan (2007) simplified the procedure by considering a trilinear monotonic force-displacement behavior. Zhao and Kwan (2003) examined the response of deep reinforced concrete coupling beams under monotonic loading. All the above studies mainly concentrated on coupling beams with moderate to low shear span ratios. Based on theoretical studies, Kwan *et al.* (2004) indicated that provision of confinement on reinforced concrete beams would increase the flexural ductility. Their study did not consider beams with equal amount of top and bottom reinforcements as in the case of coupling beams. To date, there exist limited studies on the seismic performance of coupling beams designed to non-seismic requirements.

It is the objective of this study to examine the seismic performance of coupling beams not designed for ductility. The critical design variable for the type of coupling beams as shown in Fig. 1(a) is the end shears V , see Fig. 1(b). These are introduced through the coupling between two shear walls. The coupling beams have limited structural depth (so as to facilitate the installation of services, false ceiling, etc.) and are subjected to large bending moments $\pm VL/2$, as shown in Fig. 1(b). Without the requirement on ductility, the coupling beams are heavily reinforced with the main tensile reinforcements at 3-4% typical. Pursuant to CoP 1987 (1987) clause 3.2.7 (2)(d), "the spacing of links when required to resist shear should not be less than 8 times the diameter of the link, or 75 mm whichever is the greater." Reinforcement details of the stirrups are specified through a minimum spacing to ensure ease of concreting. In practice, the typical spacing of stirrups is 150-200 mm. Furthermore, the use of 90-degree hooks not permitted in seismic detailing is also allowed.

In this study, coupling beam specimens having the above-mentioned non-seismic details were tested under cycles of push-pull action. The test data were correlated to develop an empirical relationship to estimate the ultimate drift angle of coupling beams designed without seismic provisions. This could help the engineers to assess whether the ductility of existing coupling beams are adequate to meet the ductility demand that might arise.

2. Test specimens

The eight coupling beam specimens are in 1:4 scale and with different reinforcement details. Shear span ratios are in the range of 2.5-3.5. As shown in Fig. 1(b), the specimens were assumed to be subjected to end shears V (in either direction) and fixed end moments $VL/2$, where L is the clear

span. The end shears were introduced in consideration of the wind loads and the specimens were designed according to the design code BS8110:1985 assuming rectangular sections. They were doubly reinforced with the tensile reinforcements at 3-4% typical. Due to the cyclic nature of the end shears ($\pm V$), equal amount of main reinforcements was placed at the top and bottom of the specimens. Reinforcement details of the specimens are shown in Fig. 2. In specifying the stirrup details, $\phi X@Y$ means the use of Xmm diameter stirrups at Ymm spacing.

Specimens L-A to L-E represent four of the critical coupling beams existed in the high-rise buildings in Hong Kong. The design bending moments and the design shear forces of the critical

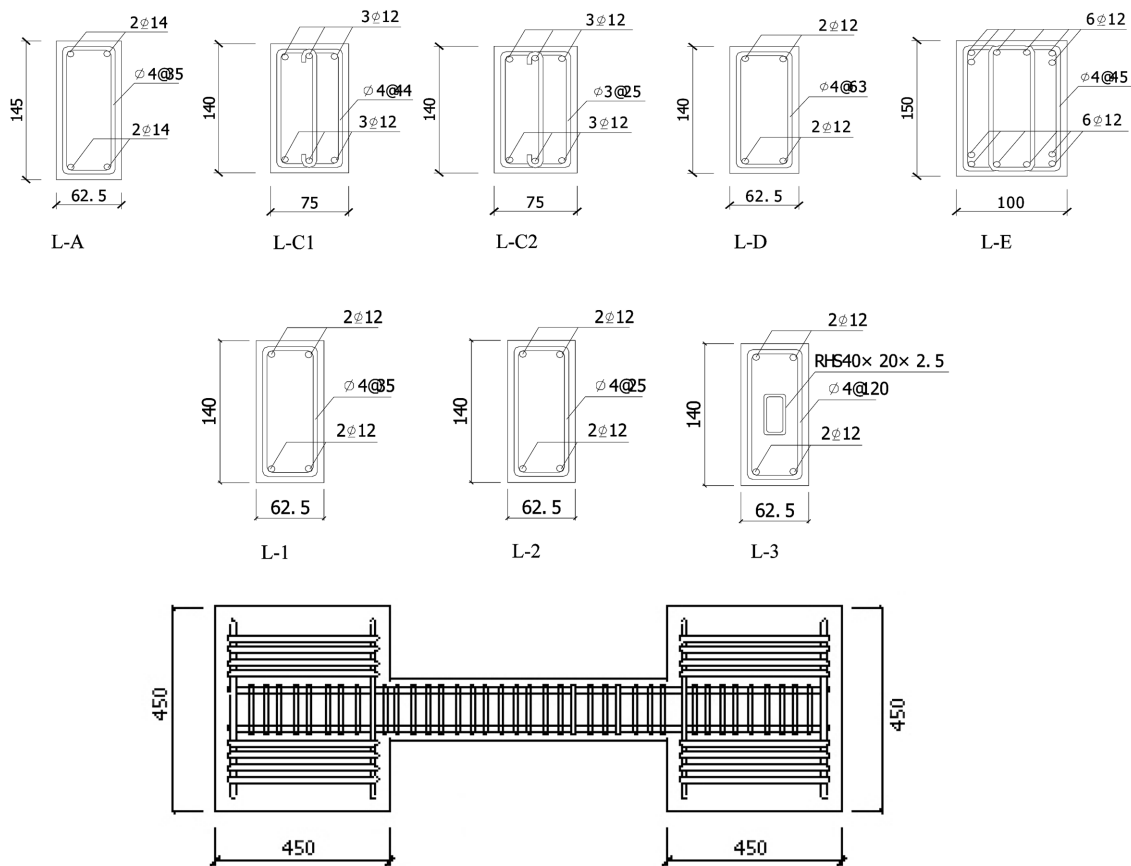


Fig. 2 Reinforcement details

Table 1 Design variables of critical coupling beams

Specimen	Dimensions and design variables in full scale		
	Breadth \times Depth (mm)	Design shear force (kN)	Design bending moment (kNm)
L-A	250 \times 580	487	731
L-C1, L-C2	300 \times 560	587	733
L-D	250 \times 560	322	483
L-E	400 \times 600	740	1295

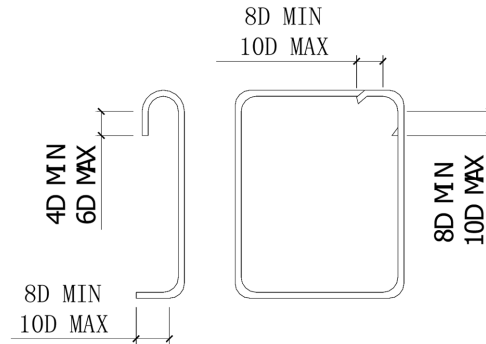


Fig. 3 Anchorage details of stirrups

Table 2 Basic characteristic of the specimens

Specimen	$B \times H$ (mm)	h (mm)	L (mm)	λ	A_{st}	ρ	Stirrups	$A_{sh}/S_t B$
L-A	62.5×145	128	750	2.9	$2\Phi 14$	3.85%	$\Phi 4$ -2legs@35	1.15%
L-C1	75×140	124	625	2.5	$3\Phi 12$	3.65%	$\Phi 4$ -3legs@44	1.15%
L-C2	75×140	124	625	2.5	$3\Phi 12$	3.65%	$\Phi 3$ -3legs@25	1.15%
L-D	62.5×140	124	750	3.0	$2\Phi 12$	2.92%	$\Phi 4$ -2legs@63	0.64%
L-E	100×150	122	875	3.5	$6\Phi 12$	5.56%	$\Phi 4$ -4legs@45	1.12%
L-1	62.5×140	124	750	3.0	$2\Phi 12$	2.92%	$\Phi 4$ -2legs@35	1.15%
L-2	62.5×140	124	750	3.0	$2\Phi 12$	2.92%	$\Phi 4$ -2legs@25	1.61%
L-3	62.5×140	124	750	3.0	$2\Phi 12$	2.92%	$\Phi 4$ -2legs@120	0.34%

coupling beams are given in Table 1A. Basic characteristics of the specimens are given in Table 1B. Here, B , H , h and L are the breadth, overall depth, effective depth and clear span. λ is the shear span ratio and is defined as half clear span divided by the effective depth. A_{st} is area of the main reinforcement, or the bottom steel as shown in Fig. 2. ρ is the amount of A_{st} expressed as a fraction of the cross-sectional area. Transverse reinforcement (or stirrup) ratio is defined as $A_{sh}/S_t B$. A_{sh} is the total area of stirrups in the transverse direction of bending and S_t is the stirrup spacing. Furthermore, all stirrups had 90-degree hooks based on standard non-seismic details as shown in Fig. 3.

Specimen L-3 has the same amount of main reinforcements as specimen L-D. It is embedded with a centrally-located rectangular hollow section (“RHS”) of 40 mm by 20 mm and 2.5 mm thickness. Specified yield strength of the rectangular hollow section is 215 MPa. In constructing the specimen, ends of the RHS were sealed to prevent any concrete from getting into the RHS. Embedded length of the RHS was 400 mm to ensure there is sufficient bond and anchorage, Harries *et al.* (2000). Shear studs were not provided and the transfer of forces between the RHS and surrounding concrete relied on the bond strength. Shear resistance of specimen L-3 is assumed to be provided by the RHS alone and flexural strength is provided by the main reinforcements only. Nominal stirrups were provided (with $A_{sh}/S_t B = 0.34\%$) only for the purpose of securing the main reinforcements.

Normal strength concrete with maximum aggregate size at 5 mm was used in all the specimens. Specimens L-A to L-E were fabricated at the same time. Specimens L-1 to L-3 were fabricated at a later time. 100 mm test cubes were prepared to estimate the cube strength of concrete, f_{cu} , for specimens L-A to L-E and L-1 to L-3 respectively. The specimens were tested at the age of 40-45 days. Measured material properties of the specimens are shown in Table 2.

3. Test setup and loading program

Tests were conducted using an existing loading frame installed in the Harbin Institute of Technology, China. It was constructed in the 70s and is similar to those used by others, for instance Nakata *et al.* (1978) and Xiao *et al.* (1986). It has been used in the testing of columns and other structural members, e.g. to assess the ductility of axially loaded reinforced concrete columns (for instance, Lam *et al.* (2003)). Fig. 4 shows the loading apparatus. To prevent the ends of the specimen from rotating, a pantograph system was used to connect the loading arm and the reaction floor, and a constant axial load (at 1% of the axial load capacity of a specimen) was applied at the top stub of the specimen by two manually controlled hydraulic jacks. This provided a double bending condition with the point of inflection at mid-height. A load cell was installed to measure the applied force V . Transducers were used to measure the relative displacements between the top and bottom stubs and the displacements within the plastic hinges.

The specimens were subjected to a series of positive and negative loading cycles. The first push cycle was used to estimate a displacement U_1 . With the loading applied using load control, the initial stiffness was estimated from the load-deformation plot. U_1 was the corresponding displacement when the stiffness estimated from the load-deformation plot was reduced by 10% from

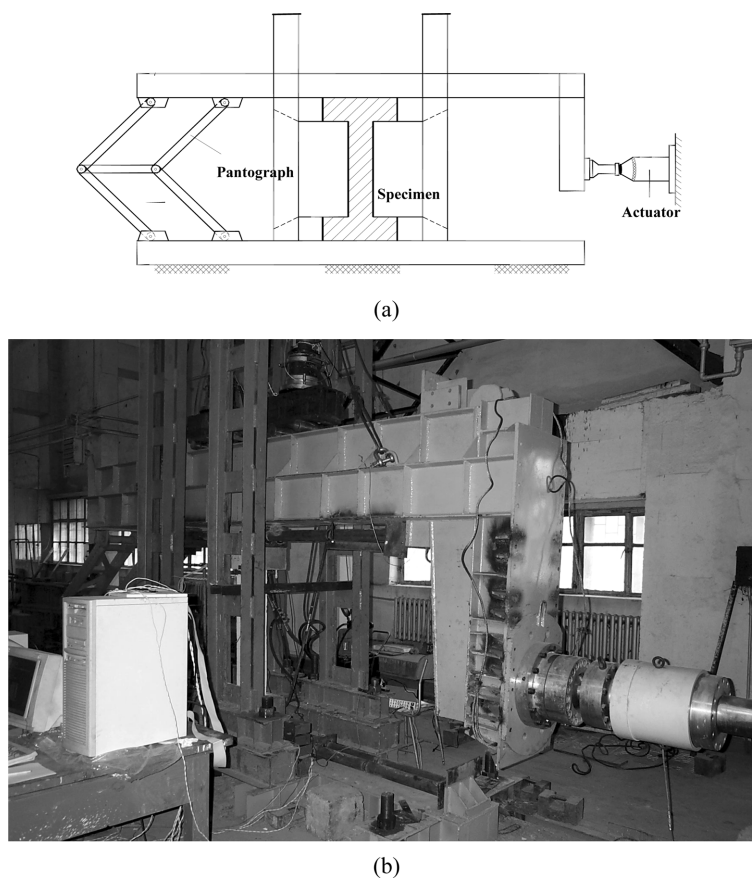


Fig. 4 Setup of the loading apparatus

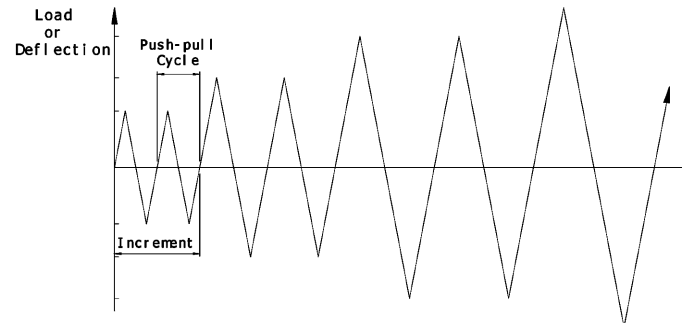


Fig. 5 Loading history

the initial value. Thereafter, the loading was applied through displacement control. Two complete cycles of push-pull loading were applied to achieve the targeted displacement δ with $\delta = U1$. The loading cycles continued with progressive increase in the displacement, see Fig. 5. The loading cycles terminated when there was more than 20% drop in the load-carrying capacity from the maximum.

4. Crack patterns and modes of failure

When subject to cycles of push-pull loading, failures of all the specimens (except specimen L-3) were mainly due to shear. Fig. 6 shows condition of the specimens at failure. Formation of cracks and the modes of failure are similar to all the specimens (except specimen L-3). Plastic hinges were formed at the two ends of the specimens. Crack patterns at the two ends of a specimen were consistent and agreed reasonable well with each other. In specimens L-A, L-E and L1, there are noticeable differences in the extent of damage at the two ends due to the spalling of concrete. During the first application of loading, the specimens exhibited a few flexural cracks within the plastic hinges at the two ends. In subsequent cycles of push-pull action, shear cracks developed. The specimens eventually failed with different degree of spalling of concrete within the plastic hinges. However, opening of the 90-degree hooks was not observed. Brief descriptions of the modes of failure of specimens L-A to L-E and L-1 to L-2 were reported in Liu *et al.* (2002a,b) respectively.

For specimens L-1 and L-2 with smaller stirrup spacing, cracks were found to be concentrated at the two ends. On the contrary, formation of cracks on specimen L-D (having the largest stirrup spacing) was more extensive and covered over the length of the specimen.

In the first few push-pull cycles, load-carrying capacity of specimen L-3 developed through the composite action between the rectangular hollow section and concrete. This suppressed the development of cracks within the plastic hinges. With progressive increase in the displacement, spalling of concrete and bond failure at the steel-concrete interface occurred at the mid-span. Due to the deterioration of the composite action, there is substantial reduction in the load-carrying capacity and the specimen has limited ductility. Shear crack were observed along the length of the specimen. This serves to indicate the importance in maintaining the composite action by providing sufficient shear resistance in the surrounding concrete.

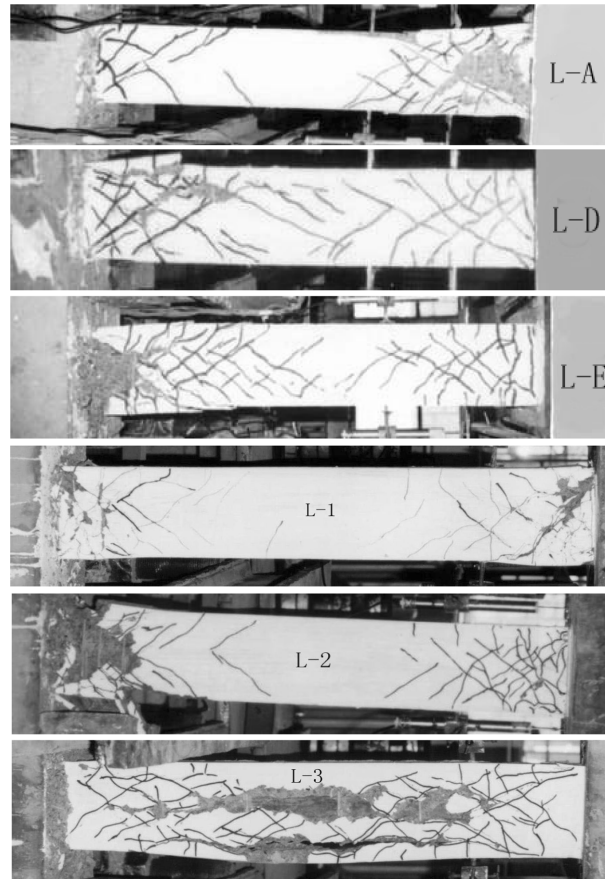


Fig. 6 Modes of failure of the specimens

5. Hysteresis behavior

Figs. 7 and 8 plot the respective hysteresis loops and load-displacement envelopes of all the specimens. In general, the specimen can only offer limited displacement ductility. Principal data of the test results are summarized in Table 3. Measured ultimate force P_m , ultimate displacement Δ_m , failure force P_u and displacement at failure Δ_u are obtained by taking the average of the values obtained from the positive and negative envelopes. For specimen L-1 and L-2, the test results in Table 3 are obtained from the negative envelopes. Failure force and displacement at failure are the corresponding values at 20 percent drop in the load-carrying capacity from the maximum. Ultimate force is the maximum strength attended in the tests.

In Table 3, displacement ductility factor is the ratio of the displacement at failure to the yield displacement. Three methods are used to estimate the yield displacements. First method denoted as “Analytical” estimates the yield displacement analytically in considering the elastic response of a cracked section. It is noted that yield forces of specimens L-A, L-C1 and L-C2 obtained by the analytical method are greater than the measured ultimate forces. We suspect that main reinforcements of these three specimens were obtained from a lot different from those used in the tensile tests. Second method denoted as “Capacity” is based on the load-carrying capacity as shown in Fig. 9.

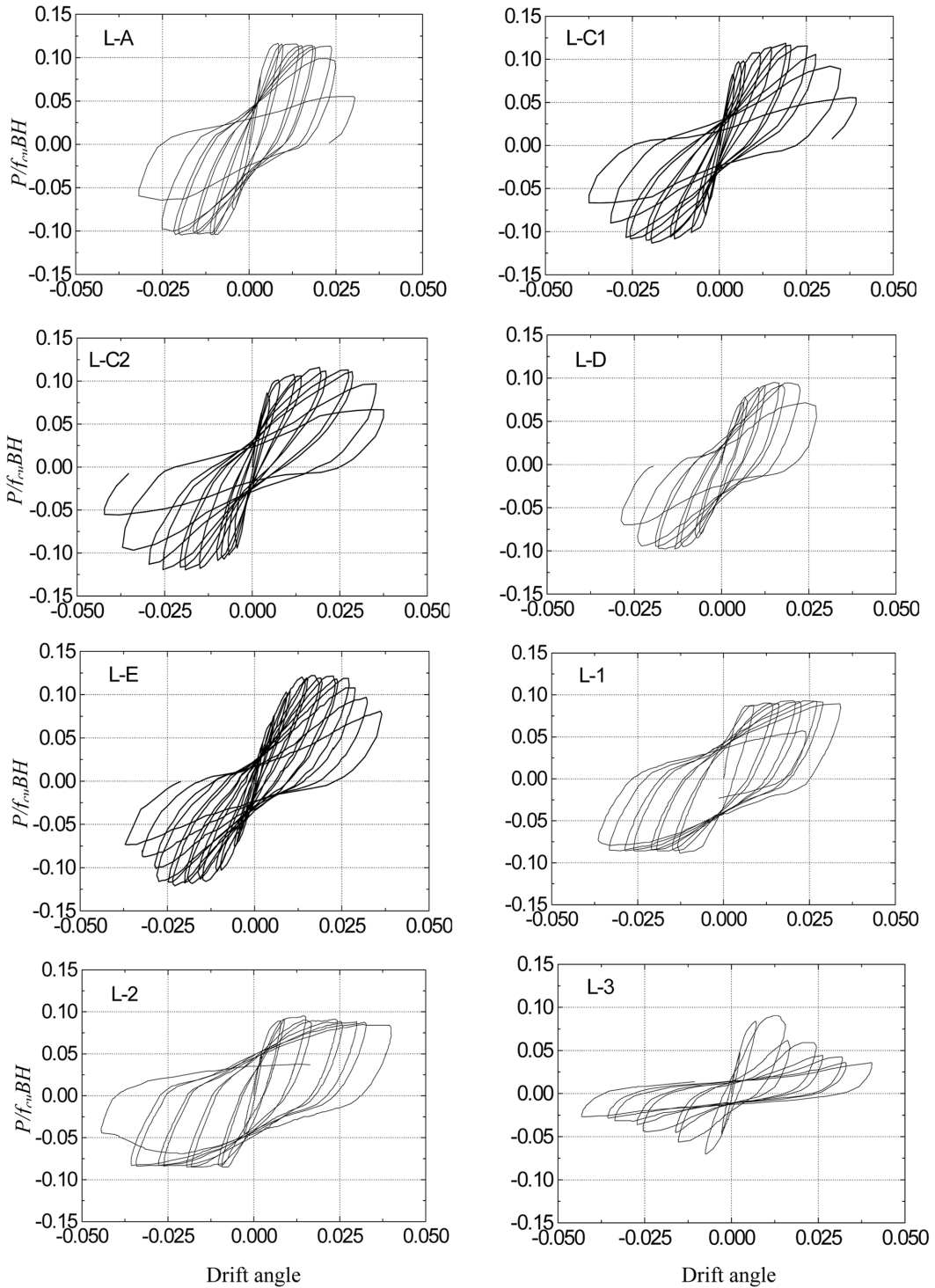


Fig. 7 Hysteresis behavior

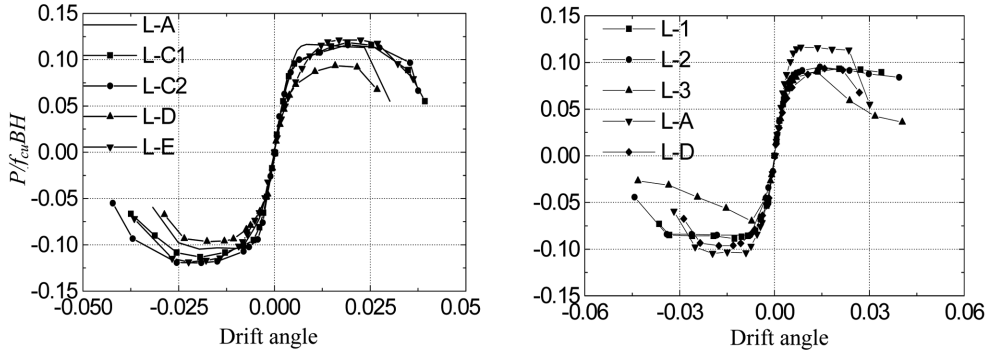


Fig. 8 Load-displacement envelopes

Table 3 Measured material properties of the specimens

Specimens		Cube strength f_{cu} (N/mm ²)	
L-A to L-E		37.3	
L-1 to L-3		38.1	
Reinforcements of L-A to L-E	Yield strength (N/mm ²)	Yield strain	Ultimate strength (N/mm ²)
$\phi 3$ steel wire	310	0.001550	429
$\phi 4$ steel wire	273	0.001365	374
$\phi 12$ bars	393	0.001965	590
$\phi 14$ bars	422	0.002110	630
Reinforcements of L-1 to L-3	Yield strength (N/mm ²)	Yield strain	Ultimate strength (N/mm ²)
$\phi 4$ steel wire	284	0.001420	391
$\phi 12$ bars	386	0.001930	582

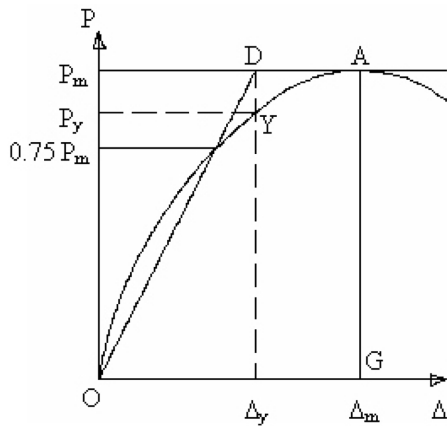


Fig. 9 Capacity method

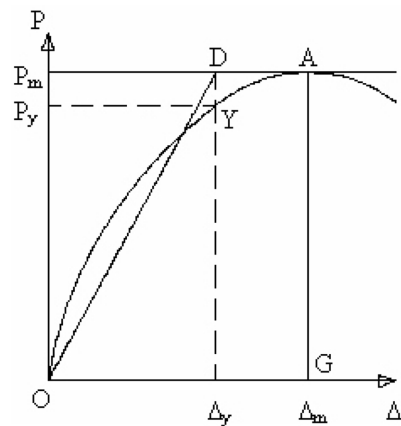


Fig. 10 Energy method

Third method denoted as “Energy” is based on an energy method as shown in Fig. 10. Yielding is estimated by equaling the area enclosed by OAG and the ODAG. Yield displacement Δ_y and yield force P_y are the corresponding values at point Y. Markedly different values could be obtained when different methods are used to estimate the displacement ductility, especially in specimens L-C1 and L-C2. Similar observations were also reported by Tassios *et al.* (1996) in estimating the displacement ductility of coupling beams. As an alternative, the ultimate drift angle is introduced and is defined as the displacement at the failure force divided by the clear span of the specimen. It provides a more consistent indicator in ranking the seismic performance of coupling beams.

The following are observed when comparing the displacement ductility and ultimate drift angles of the various specimens:

1. In comparing the ultimate drift angles, specimens L-C1, L-C2 and L-E perform better than specimens L-A and L-D. In reviewing the reinforcement detail, it seems that the use of 3- or 4-legged stirrups has some advantage over the use of single (2-legged) stirrups.
2. Specimen L-A performs better than specimen L-D by about 20%. Notwithstanding stirrup spacing of specimen L-D is 250 mm in full scale, some degree of ductility could still be achieved at large stirrup spacing.
3. Main reinforcements in specimens L-A is 32% more than that specified in specimen L-1. This leads to a 23% increase in the ultimate force P_m . However, there is substantial reduction in both the ultimate drift angle and displacement ductility factor by 28% and 30% respectively. This agrees well with the general principle in that the use of heavily reinforced beams may seriously reduce the ductility and is therefore undesirable for seismic resistance.
4. Reinforcement details of specimens L-C1 and L-C2 are identical, except the stirrup spacing. Seismic performance achieved by these two specimens is similar. In maintaining the same transverse reinforcement ratio $A_{sh}/S_t B$, there is an about 10% increase in the displacement ductility factor and ultimate drift angle when reducing the stirrup spacing from 44 mm to 25 mm (43% reduction). It seems that the primary objective on the design of this type of coupling beams is to satisfy the transverse reinforcement ratio $A_{sh}/S_t B$. Although the stirrup spacing should also not be greater than a certain limiting value, this was not considered in the study.
5. Specimen L-E produces the smallest displacement ductility as compared with the other specimens. This specimen is heavily reinforced with 5.56% main reinforcement, and having the largest shear span ratio at 3.5. Notwithstanding having similar transverse reinforcement ratio and stirrup spacing as specimen L-C1, the displacement ductility is only 60-70% of specimen L-C1. This demonstrates the adverse effect in using heavily reinforced section.
6. Apart from having different stirrup spacing, specimens L-1, L-2 and L-D have the same reinforcement details. When the stirrup spacing is reduced from 63 mm (specimen L-D) to 35 mm (specimen L-1), the ultimate drift angle and displacement ductility factor increase by 42% and 71% respectively. When the stirrup spacing is further reduced to 25 mm (specimen L-2), there is no obvious gain in either the ultimate drift angle or displacement ductility factor.
7. The use of smaller stirrup spacing is essential in the case of specimen L-3 in order to maintain the composite action throughout the loading history.

6. Energy dissipation

The normalized total dissipated energy ($E/P_y \Delta_y$) and normalized dissipated energy at the last cycle

Table 4 Test results

Specimen		L-A	L-C1	L-C2	L-D	L-E	L-1	L-2	L-3
Yield force P_y (kN)	Analytical	38.19	45.69	45.69	25.42	58.89	25.42	25.42	25.42
	Capacity	32.28	37.88	38.20	25.70	58.21	26.85	26.44	22.93
	Energy	32.78	39.06	40.08	26.02	58.04	26.89	26.00	23.07
Yield displacement Δ_y (mm)	Analytical	4.48	3.08	3.08	4.11	6.39	4.11	4.11	4.11
	Capacity	4.28	3.49	3.48	5.03	8.46	4.18	4.48	4.08
	Energy	4.42	4.66	4.45	5.33	8.43	4.30	4.38	4.12
Measured Ultimate force P_m (kN)		37.23	45.44	46.11	31.01	67.12	30.30	30.00	26.77
Ultimate displacement Δ_m (mm)		6.52	12.02	11.97	12.55	19.66	12.45	12.20	7.71
Failure force P_u (kN)		29.79	36.35	36.86	24.53	53.71	23.62	22.64	21.49
Displacement at failure Δ_u (mm)		20.04	19.91	21.84	19.66	27.64	27.87	28.67	13.03
Ultimate drift angle		26.7×10^{-3}	31.9×10^{-3}	35.0×10^{-3}	26.3×10^{-3}	31.6×10^{-3}	37.2×10^{-3}	38.2×10^{-3}	17.4×10^{-3}
Displacement ductility factor	Analytical	4.47	6.46	7.09	4.78	4.33	6.78	6.96	3.17
	Capacity	4.68	5.70	6.27	3.91	3.27	6.67	6.40	3.20
	Energy	4.53	4.27	4.91	3.69	3.28	6.48	6.55	3.16

Table 5 Total energy dissipated

Specimen	L-A	L-C1	L-C2	L-D	L-E	L-1	L-2
Total energy up to failure (KNm)	5.14	5.08	5.40	3.24	12.30	6.73	8.14
Normalized total energy $E/P_y\Delta_y$	35.5	27.9	30.3	23.3	25.1	58.3	70.3

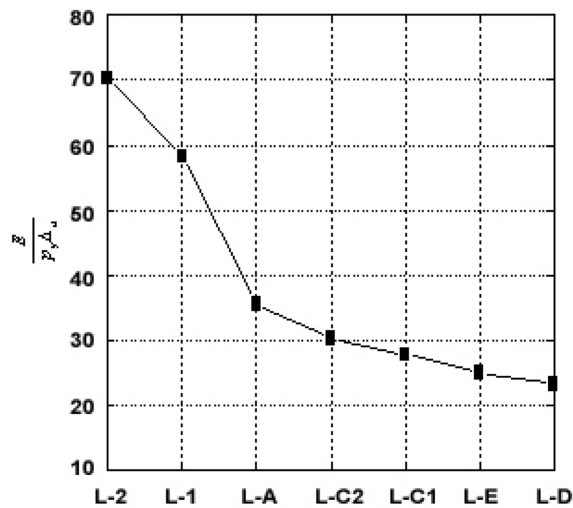


Fig. 11 Total energy dissipation

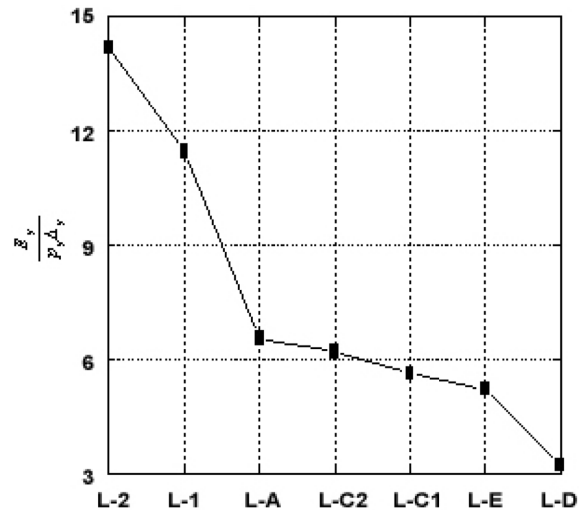


Fig. 12 Energy dissipated at the last cycle

$(E_p/P_y\Delta_y)$ of the specimens are summarized in Tables 4 and 5 respectively. Yield force P_y and the corresponding yield displacement Δ_y are estimated based on the Energy Method. Total dissipated energy E is estimated by summing up the areas enclosed by the complete hysteresis loops, whereas dissipated energy at the last cycle E_p is the corresponding enclosed area of the last hysteresis loop

before failure. Figs. 11 and 12 compare the normalized energies achieved by the various specimens. In general, performance of the specimens in terms of total dissipated energy or dissipated energy at the last cycle is similar.

$E/P_y\Delta_y$ is increased by 150% when the stirrup spacing is reduced from 63 mm (specimen L-D) to 35 mm (specimen L-1), but is only increased by 21% when the stirrup spacing is further reduced to 25 mm (specimen L-2). Main reinforcement in specimen L-A is 32% more than that in specimen L-1. This leads to a 64% reduction in $E/P_y\Delta_u$. The comparisons are consistent with the observations obtained from the various hysteresis behaviors. This can be explained by the well established shear-resisting mechanisms, Park and Paulay (1975). When subjected to repeated load reversals, all shear-resisting mechanisms other than the truss action deteriorate and are not effective to resist shear. To maintain the ductile behavior of the type of coupling beams considered in this study, we need to ensure that the truss action will not deteriorate under repeated load. In particular, it is essential to design the coupling beams with closely spaced stirrups and proper detailing.

7. Deformation

Possible sources of deformation include flexural displacement, shear displacement and displacement due to bond slip. Displacement transducers were installed at one end of a specimen to measure the displacement in the vicinity of the plastic hinge. In the study, the measurement points were setup so as to estimate the flexural displacement only. It is assumed that displacements at the ends of a specimen are identical so that the total deformation within the plastic hinges is simply twice the value obtained from the estimation.

Based on the two measurements δ_{1f} and δ_{2f} taken at a distance H from one end of the specimen, as shown in Fig. 13, flexural displacement Δ_f can be calculated by the following equation.

$$\Delta_f = 2 \times \left[\int_0^H \phi_y y dy + \theta(L/2 - H) \right] = \frac{(L - H)(\delta_{1f} - \delta_{2f})}{h_0} \tag{1}$$

where y is the longitudinal distance measured from one end of the specimen, ϕ_y is the yield curvature and h_0 is the distance measured center-to-center between the bottom and top

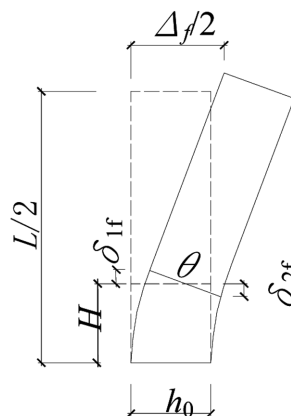


Fig. 13 Flexural displacement within the plastic hinge

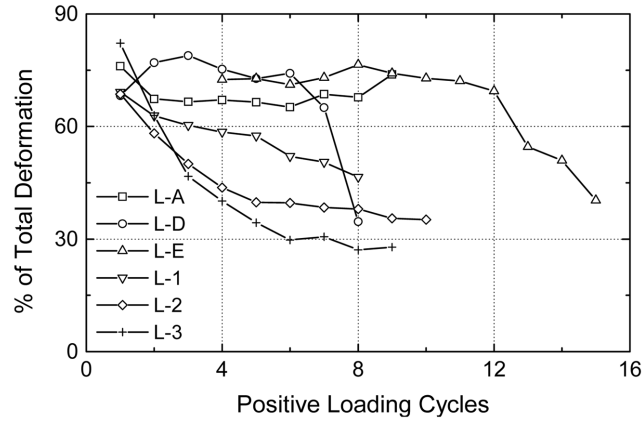


Fig. 14 Relative flexural displacement

reinforcements. Eq. (1) does not take into account possible axial elongation of the coupling beams (for instance see Park and Paulay (1975)) which is considered not significant in this study.

Fig. 14 shows the relative flexural displacement (expressed as percentage of the total deformation) within the plastic hinge against the number of positive loading cycles of six specimens. Apart from specimen L-A, all specimens exhibit substantial reduction in the relative flexural displacement when approaching failure. For specimen L-A, the relative flexural displacement remains the same throughout the loading cycles, with an averaged value at 69%. For specimen L-D, the relative flexural displacement is about 74% in the first 6 cycles, and drops to 35% at the 8th cycle. Similar to specimen L-D, the relative flexural displacement of specimen L-E decreases rapidly when approaching failure at the 15th cycle to about 40%. As for specimens L-1, L-2 and L-3, the relative flexural displacement decreases with increasing number of loading cycles. The relative flexural displacement is about 40% at failure for specimens L-1 and L-2.

From the observed damage under progressive increase in the loading cycles, there was no obvious sign of bond slip. Therefore, the total deformation should only comprise shear and flexural displacements. In all the tests, reduction in flexural displacement would imply an increase in the shear displacement. As shown in Fig. 14, when approaching failure, there is substantial reduction in the flexural displacement. Hence, there is substantial increase in the shear displacement. This reaffirms that the modes of failure of the various specimens are due to shear.

8. Empirical relationship for ultimate drift angle

In order to develop an empirical formula to predict the ultimate drift angle of non-ductile coupling beams, test data obtained from this study (except specimen L-3) are correlated.

Based on the observations obtained from the test results, the main reinforcement ratio ρ , the shear span ratio λ and the transverse reinforcement ratio $A_{sh}/S_t B$ are identified as the main controlling factors affecting the ultimate drift angle θ . After examining several mathematical expressions, an empirical relationship is proposed and is in form of

$$\theta = 0.1188(A_{sh}/S_t B)^2/(\lambda\rho^2) + 0.0274 \quad (2)$$

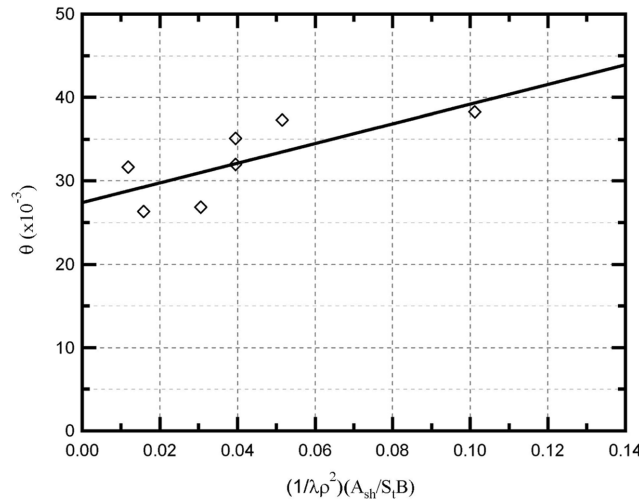


Fig. 15 Variation of θ against $(A_{sh}/S_t B)^2/(\lambda \rho^2)$

Table 6 Energy dissipated at the last cycle

Specimen	L-A	L-C1	L-C2	L-D	L-E	L-1	L-2
Total energy of the last cycle (KBm)	0.93	1.00	1.06	0.72	1.59	1.33	1.65
Normalized energy of the last cycle $E_p/P_y \Delta_y$	6.57	5.64	6.23	5.24	3.25	11.47	14.20

Eq. (2) is obtained using the nonlinear regression technique. Fig. 15 plots the variation of the ultimate drift angle against $(A_{sh}/S_t B)^2/(\lambda \rho^2)$. Values predicted by the empirical relationship generally agree well with the experimental data. Lastly, applicable range of the empirical relationship is limited to normal strength concrete, moderate shear span ratio in the range of 2.5-3.5 and with the lateral reinforcement ratio within the range of $0.5\% < A_{sh}/S_t B < 1.6\%$.

9. Conclusions

Eight coupling beam specimens not designed for ductility were tested under cycles of push-pull action. The specimens are in 1:4 scale with the shear span ratios in the range of 2.5-3.5. Characteristics of the specimens include high main reinforcement ratio, about 3-4%, and large stirrup spacing with 90-degree hooks. Displacement ductility of specimens with large stirrup spacing (≥ 140 mm) is in the range of 3 to 5. At the initial stage of the loading history, there exists considerable flexural deformation. When approaching failure, there is substantial increase in the shear deformation. This affirms that the modes of failure of the specimens with moderate shear span are due to shear.

Based on the test data, an empirical relationship is proposed to estimate the ultimate drift angle of coupling beams not designed for ductility. Applicable range of the empirical relationship should be limited to the class of coupling beams considered in the study for normal strength concrete, moderate shear span ratio in the range of 2.5-3.5 and lateral reinforcement ratio within the range of $0.6\% A_{sh}/S_t B < 1.6$.

Acknowledgements

The authors are grateful to the financial supports from the Research Grants Council of Hong Kong (RGC No: PolyU 5038/99E).

References

- ACI 318-02. Building Code Requirements for Structural Concrete. Reported by ACI Committee 318, ACI.
- Aycardi, L.E., Mander, J.B. and Reinhorn, A.M. (1994), "Seismic Resistance of Reinforced Concrete Frame Structures Designed Only for Gravity Loads, Experimental Performance of Subassemblages", *ACI Struct. J.*, **91**(5), 552-563.
- Barney, G.B., Shiu, K.N., Rabba, B.G., Fiorato, A.E., Russell, H.G. and Corle, W.G. (1980), *Behavior of Coupling Beams under Load Reversals*. Research and Development Bulletin RD068.01, PCA, Research and Development/Construction Technology Laboratories.
- Bracci, J.M. and Reinhorn, A.M. (1996), Shaking Table Testing of a 1:3 Scale R/C Frame Model. *EURODYN'96*.
Code of Practice for Structural Use of Concrete – 1987, Buildings and Lands Department, Hong Kong.
- Durrani, A.J., Du, Y. and Luo, Y.H. (1995), "Seismic resistance of nonductile slab-column connections in existing flat-slab buildings", *ACI Struct. J.*, **92**(4), 479-487.
- Harries, K.A., Gong, B. and Shahrooz, B.M. (2000), "Behavior and design of reinforced concrete, steel, and steel-concrete coupling beams", *Earthq. Spectra*, **16**(4), 775-799.
- Harries, K.A. (2001), "Ductility and deformability of coupling beams in reinforced concrete coupled walls", *Earthq. Spectra*, **17**(3), 457-478.
- Hindi, R.A. and Hassan, M.A. (2004), "Shear capacity of diagonally reinforced coupling beams", *Eng. Struct.*, **27**, 1437-1446.
- Hindi, R. and Hassan, M. (2007), "Simplified trilinear behavior of diagonally reinforced coupling beams", *ACI Struct. J.*, 199-206.
- Kwan, A.K.H., Au, F.T.K. and Chau, S.L. (2004), "Theoretical study on effect of confinement on flexural ductility of normal and high-strength concrete beams", *Mag. Concrete Res.*, **56**(5), 299-309.
- Lam, S.S.E., Wu, B., Wong, Y.L., Wang, Z.Y., Liu, Z.Q. and Li, C.S. (2003), "Drift capacity of rectangular reinforced concrete columns with low lateral confinement", *J. Struct. Eng.*, ASCE, **129**(6), 733-742.
- Liu, Z.Q., Lam, S.S.E. and Wu, B. (2002a), Seismic Performance of Non-ductile Coupling Beams. *Proc. of the Structural Engineering World Congress (SEWC 2002)*, Oct. 9-12, 2002, Yokohama, Japan.
- Liu, Z.Q., Lam, S.S.E., Wu, B. and Wong, Y.L. (2002b), Ultimate Drift Ratio of Non-ductile Coupling Beams. *Proc. of Advances in Building Technology (ABT2002)*, Dec. 4-6, 2002, Hong Kong.
- Nakata, S., Sproul, T. and Penzien, J. (1978), *Mathematical Modelling of Hysteresis Loops for Reinforced Concrete Columns*. Report No. UCB/EERC-78/11.
- NZS 3101:2006: Part 1. The Design of Concrete Structures, Standards New Zealand, Wellington.
- Pam, H.J., Su, R.K.L., Lam, W.Y., Li, J., Au, F.T.K., Kwan, A.K.H. and Lee, P.K.K. (2002), Designing Coupling Beams and Joints in Concrete Buildings for Improved Earthquake Resistance. *Proc. of Recent Developments in Earthquake Engineering*, HKIE Structural Division, 17 May 2002, 91-105.
- Park, R. and Paulay, T. (1975), *Reinforced Concrete Structures*, John Wiley & Sons.
- Paulay, T. (1971), "Coupling beams of reinforced concrete shear walls", *J. Struct. Div.*, ASCE, **97**(3), 843-861.
- Paulay, T. and Binney, J.R. (1974), "Diagonally reinforced coupling beams of shear walls", Paper no 26, *ACI Publication SP-42*, **2**, 579-598.
- Paulay, T. (2002), "A Displacement-focused Seismic Design of Mixed Building System", *Earthq. Spectra*, **18**(4), 689-718.
- Tassios, T.P., Moretti, M. and Bezas, A. (1996), "On the behavior and ductility of reinforced concrete coupling beams of shear walls", *ACI Struct. J.*, **93**(6).
- Subedi, N.K. (1991a), "RC-coupled shear wall structures. I: Analysis of coupling beams", *J. Struct. Eng.*, ASCE,

- 117**(3), 667-680.
- Subedi, N.K. (1991b), "RC-coupled shear wall structures. II: Ultimate strength calculation", *J. Struct. Eng.*, ASCE, **117**(3), 681-698.
- Xiao, Y., Tomli, M. and Sakino, K. (1986), "Experimental study on design method to prevent shear failure of reinforced concrete short circular columns by confining in steel tube", *Trans. Japan Concrete Inst.* **8**, 535-542.
- Xu, Y.L., Ko, J.M., Chau, K.T., Lam, S.S. and Wong, Y.L. (2001), "Research of earthquake engineering in Hong Kong: current status and future challenge", *Earthquake Engineering Frontiers in the New Millennium*, Spencer & Hu (eds), Swet & Zeitlinger, 77-99.
- Zhao, Z.Z. and Kwan, A.K.H. (2003), "Nonlinear Behavior of Deep Reinforced Concrete Coupling beam", *Struct. Eng. Mech.*, **15**(2), 181-198.

Notation

The following symbols are used in this paper:

- A_{sh} : total cross-sectional area of stirrups
 A_{st} : area of main reinforcements in the tensile zone
 B : breadth of coupling beam
 E : total dissipated energy
 E_p : dissipated energy at last cycle
 f_{cu} : cube strength of concrete
 H : overall depth of a cross-section
 H, h : effective depth of a cross-section
 L : clear span of coupling beam
 P_m : measured ultimate force
 P_y : yield force
 S_t : stirrup spacing
 P, V : shear force
 Δ_f : flexural displacement
 Δ_y : yield displacement
 θ : ultimate drift angle
 λ : shear span ratio defined as half clear span divided by effective depth
 ρ : ratio of main reinforcements in tensile zone to cross-sectional area